A Numerical Study of the Mesoscale Atmospheric Circulation Observed during a Coastal Upwelling Event on 23 August 1972. Part I: Sensitivity Studies

ARTHUR PAUL MIZZI

National Center for Atmospheric Research,[1] Boulder, CO 80307

ROGER A. PIELKE

Colorado State University, Fort Collins, CO 80523

(Manuscript received 27 November 1982, in final form 25 June 1983)

ABSTRACT

A numerical model is used to study the effect of an ocean surface temperature gradient on the mesoscale atmospheric circulation. The model is initialized with atmospheric data from 23 August 1972 over the central Oregon coastal zone. After the initial fields are balanced the model is integrated for 24 h and the results are analyzed and compared with observations.

Both our analysis and the observations show the development of a coastal, low-level jet after sunset. An analysis of the mesoscale wind component shows that this jet is related to the sudden change in the top of the boundary layer and the increased thermal stratification after sunset.

Turbulent mixing and terrestrial heating are found to overwhelm the inland advection of marine air so that there is no daytime thermal front over the land. After sunset the front moves inland in response to long-wave radiation cooling and stabilization of the lower atmosphere.

Our analysis shows that the warm zone to the east of the thermal front and the cool zone to the west are maintained by turbulent mixing and increased stability respectively. These results differ from the explanation of Estoque who suggested the warm zone is maintained by reduced mixing while the cool zone is maintained by strong mixing.

Finally, during the day the ocean surface temperature gradient weakens the longshore component of the wind due to increased atmospheric stability and higher ocean surface temperatures to the west.

1. Introduction

This is the first in a two-part series of papers which examine the mesoscale atmospheric circulation in the coastal region. This paper deals with the effect of the mesoscale spatial gradient of ocean surface temperature on the atmospheric circulation. The second part will examine the effects of topography and spatially uniform changes in the mean sea surface temperature on the mesoscale atmospheric circulation.

During the summers of 1972 and 1973, the Coastal Upwelling Experiments, CUE I and CUE II, were conducted along the central coast of Oregon. These experiments were major field projects of CUEA, the NSF–IDOE sponsored Coastal Upwelling Ecosystems Analysis Program. CUEA is composed of two subprograms dealing with the biological and physical aspects of the ecosystem. Each subprogram had its own observational and theoretical component. The research presented here, although not directly involved with CUEA, relies heavily upon its research, observations, and conclusions. Specifically this study will examine and seek to explain the following features observed during CUE I on 23 August 1972:

- The sea breeze front that penetrated more than 60 km inland and the distinct wind maximum that followed the front inland.
- The lower level sea breeze circulation that was confined within the planetary boundary layer (PBL) and the upper level return flow immediately above the boundary layer.
- The low-level longshore jet that was observed to peak in the late evening just inland from the coast.

This paper examines these mesoscale[2] features with the aid of a mesoscale atmospheric model.[3] Since this numerical atmospheric model has been previously discussed in the literature a description will not be presented here. For a detailed discussion of this model the interested reader should refer to Mahrer and Pielke

[1] The National Center for Atmospheric Research is sponsored by the National Science Foundation.

[2] For the purpose of this paper "mesoscale" refers to marine and atmospheric features with length scales on the order of 50–100 km.

[3] The atmospheric model used in this study was formerly referred to as the University of Virginia mesoscale model.

(1978) and Pielke and Mahrer (1978). The two-dimensional version of the atmospheric model is used in this study in order to reduce computing costs and because the three-dimensional system along the Oregon coast is adequately described with two dimensions as pointed out by Mak and Walsh (1976). The location of the two-dimensional grid and its surrounding topography is presented in Fig. 1. For this study the model atmosphere is coded with 19 vertical levels and 96 horizontal grid points. The grid is stretched in both coordinates to provide the greatest resolution at the surface within 100 km to either side of the coast. The horizontal and vertical grid structure is presented in Tables 1 and 2 respectively. Table 2 also contains the initial profiles of potential temperature θ and specific humidity q. The remaining sections of this paper discuss model initialization and results from the flat grid simulations. Several concluding remarks are presented in the final section.

2. Model initialization

The atmospheric model is initialized with data from the CUE I special observation period. Johnson and O'Brien (1973) present a detailed analysis of these observations. As can be seen in Fig. 2 the synoptic conditions over the western United States were particularly conducive to coastal upwelling since the large scale flow was predominantly from the north on 23 August 1972. This day was chosen for the following simulations since the original goal of this study was to examine the effect of coastal upwelling on the mesoscale atmospheric circulation. The results of the coupled atmosphere–ocean model experiments, reported by Mizzi (1982), supported the conclusions of Clancy *et al.* (1979), in that upwelling was shown to have a negligible effect upon the mesoscale circulation for time scales on the order of 24 h. This result was attributed to the small spatial scale of intense upwelling (8 km). Consequently, the emphasis of the research was changed to that of explaining the observed mesoscale features reported in the introduction. For a more detailed discussion of the coupled model experiments see Mizzi (1982).

As a part of the CUE I special observation period, vertical soundings of temperature and dew point temperature were made at Newport, Oregon. Generally, these soundings were made to a height of 4.0 km. Pibal measurements were also taken at three sites along the

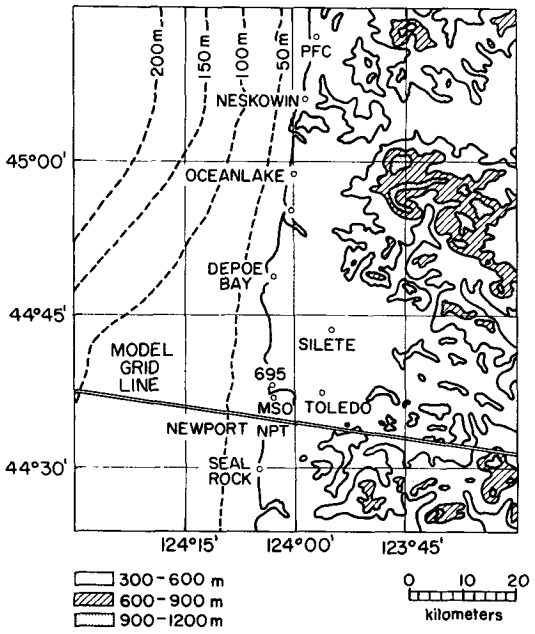

FIG. 1. A topographic map of central Oregon displaying the Coast Range and the model grid line.

TABLE 1. The horizontal grid structure of the model atmosphere.

Grid cell (i)	Grid increment (km)	Range (km)
1–21	Δx = 16.0 to 4.0	−300 to 104
22–71	Δx = 4.00	−100 to 100
72–96	Δx = 4.0 to 16.0	104 to 300

Variable grid assignments are made from $\Delta x(i) = ai^2 + bi + c$ where

$$a = -0.3; \quad b = 16.6; \quad c = -316.3 \quad \text{for} \quad (1 \leqslant i \leqslant 21)$$

and

$$a = 0.16; \quad b = -18.7; \quad c = 621.1 \quad \text{for} \quad (72 \leqslant i \leqslant 96).$$

TABLE 2. The vertical grid structure of the model atmosphere with the initial profiles of potential temperature θ and specific humidity q for various heights above mean sea level.

Model level	z (m)	P (10^2 Pa)	θ (K)	$q \times 10^{-3}$
19	10000	286.66	339.95	0.03
18	8000	378.79	335.51	0.12
17	6000	492.45	330.04	0.46
16	5000	558.40	326.61	0.60
15	4500	594.13	321.55	1.67
14	4000	631.80	318.90	3.97
13	3500	671.57	315.52	3.88
12	3000	713.62	311.57	3.79
11	2500	758.09	307.63	3.15
10	2000	805.08	304.04	2.21
9	1500	854.73	300.03	2.11
8	1000	906.98	297.39	4.31
7	700	939.47	297.33	4.84
6	500	961.71	295.47	7.64
5	300	984.50	293.49	8.16
4	200	996.15	290.32	8.63
3	100	1007.99	287.90	9.10
2	50	1013.96	287.50	9.95
1	10	1018.76	287.26	10.46

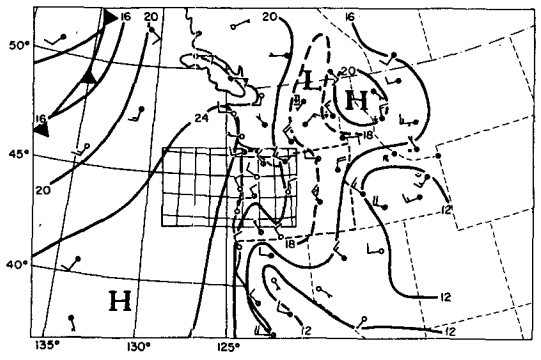

FIG. 2. The surface synoptic pattern for 25 August 1972, at 0000 GMT (O'Brien, 1972).

model grid line (Newport, Ellmaker and Corvallis). This data set was supplemented with National Weather Service (NWS) observations at Salem, Oregon, in order to derive the initial atmospheric profiles used in this study. The initial profiles are constructed from CUE I data when available. Missing data are obtained by linearly correlating the observation at Newport to simultaneous observations at Salem. The following procedures are used to correlate the various data types:

- The potential temperature at missing levels is obtained by statistically correlating the observed profile at Newport to that at Salem with the methods of linear regression. This procedure yields a regression coefficient of 0.99 and a mean scatter of 1.38 K. Unfortunately, the small sample size limits general applicability of the regression equation.
- The specific humidity at missing levels is obtained by linearly correlating the vertical gradient of the missing data to the observed gradient at Salem. The procedure used for reconstructing the potential temperature profile is not applicable since it supplies negative values of specific humidity.
- The horizontal wind components at missing levels above the PBL are obtained in the same manner to that described for completing the specific humidity profile.

These procedures are used to derive the initial data set composed of the vertical profiles of potential temperature, specific humidity and the horizontal wind components. It should be noted that the horizontal wind profile is initially required to maintain an Ekman balance within the PBL as described by Pielke and Mahrer (1978). The Ekman balance is forced by an estimate of the geostrophic wind at the top of the PBL.

As a result of the derived initial fields and the dual nature of the model domain, half land and half water, the atmospheric fields of mass and velocity are initially out of balance. This situation results in temporally damped inertia oscillations. In order to minimize the effect of these oscillations separate Ekman solutions are computed for the terrestrial and maritime atmosphere. The model atmosphere dynamically adjusts these fields for a 12 h period without thermal forcing. It is apparent from Fig. 3 that the bulk of the adjustment occurs during the first 12 h of the initialization period. This figure also shows that longer adjustment periods would have little effect upon the evolution of the initial state of the atmosphere.

In earlier experiments, an adjustment period of 44 h was used to essentially eliminate the inertial oscillations. However, later experiments demonstrated that after several hours of heating, the velocity fields are independent of the length of the adjustment period, while the thermodynamic field is only slightly dependent upon the time duration of the unforced adjustment. These results may be seen from a comparison of Fig. 4a–c. In light of these results, a 12 h adjustment period is considered adequate. It should be noted that in these and all subsequent figures the coast is located at the origin. The land area is located between 0 and 300 km while the ocean is located between 0 and −300 km.

During the CUE I observation period, no measurements of the soil thermal structure were made. Fortunately, previous experiments have shown that the sea breeze circulation exhibits little sensitivity to the temperature profile within the soil (McCumber and Pielke, 1981). For this reason, and due to the lack of data, the following method is used to derive the initial soil temperature profile as presented in Table 3:

- The mean soil surface temperature for central Oregon is obtained from available climatological data.
- The curve for a typical soil temperature profile,

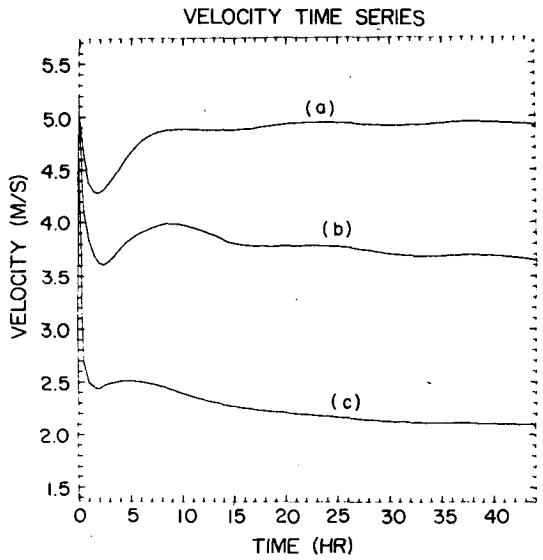

FIG. 3. Time series of the wind speed showing the convergence of the unforced atmosphere toward a balanced state at (a) Marine grid point (92 km offshore), (b) coastal grid point and (c) terrestrial grid point (92 km inland).

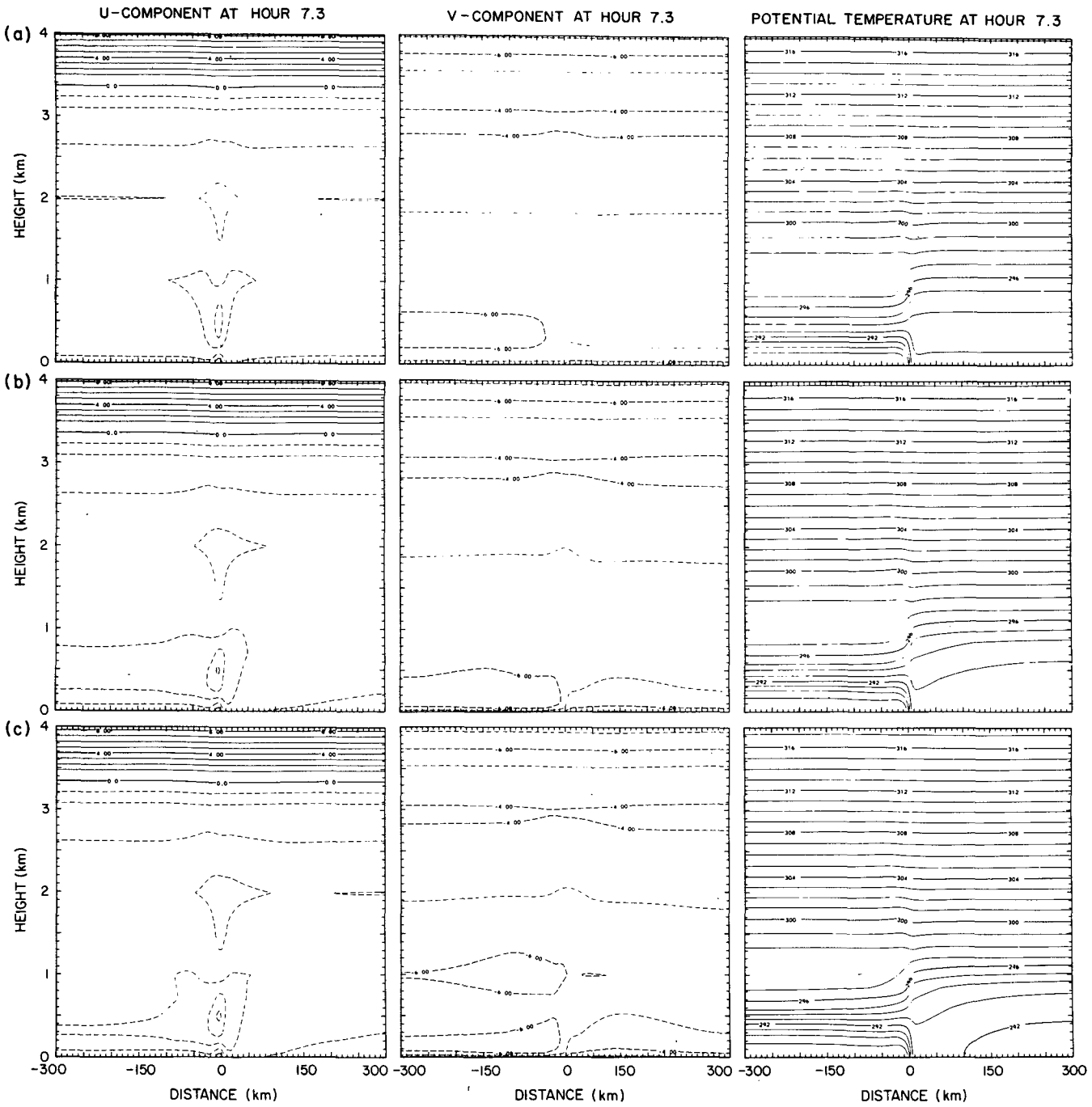

FIG. 4. The x–z contours of the u, v, and θ fields for various durations of unforced adjustment (contour intervals, 1 m s^{-1} and 1 K) for (a) No adjustment period, (b) 22 h adjustment period and (c) 44 h adjustment period.

from O'Neil, Nebraska (Lettau and Davidson, 1957), is fitted to the climatological mean for Oregon.

The specification of the remaining atmospheric parameters is either dependent upon the time of year, the geographic location or commonly accepted values from the literature. These parameters are presented in Table 4.

3. Model simulations and results

Two model simulations are discussed in this section. The first serves as a control experiment which is used to examine the geophysical forcing behind the mesoscale features reported in Section 1. For this simulation the ocean surface temperature is spatially uniform. The second experiment examines the influence

TABLE 3. The initial soil temperature profile, used as input to the slab soil segment of the atmospheric model.

Layer	Depth (m)	Temperature (K)
1	0.05	284.81
2	0.10	286.15
3	0.15	287.51
4	0.20	288.49
5	0.25	288.87
6	0.30	288.96
7	0.35	289.01
8	0.40	288.93
9	0.45	288.91
10	0.50	288.86
11	0.55	288.81
12	0.60	288.76
13	0.65	288.71
14	0.70	288.69
15	0.75	288.69
16	0.80	288.57
17	0.85	288.57
18	0.90	288.57
19	0.95	288.57

of a mesoscale gradient of the sea surface temperature as might be expected from coastal upwelling. The ocean temperature gradient was predicted with time invariant atmospheric forcing by the numerical model of coastal upwelling described by Thompson (1974).

a. *The control experiment*

In this experiment the ocean surface temperature is spatially uniform at 289 K and the results are displayed in Fig. 5.

During the day a longshore, jetlike feature develops west of the coast. Elliott and O'Brien (1977) report a similar feature observed along the Oregon coast during the CUE II field program. This phenomenon results from the combined effects of baroclinity and friction as discussed below. The baroclinity, which is created by the inland advection of marine air and terrestrial heating, forces the longshore flow to accelerate as geostrophic adjustment is induced by the mesoscale horizontal temperature gradient. McNider (1981) discusses the development of the low-level jet over sloping terrain through an analysis of the thermal wind equation. By applying this analysis to the coastal zone it can be demonstrated that the intensity of the northerly jet should increase with time due to increased baroclinity from terrestrial warming to the east, such as occurs over inland Oregon.

TABLE 4. The specification of descriptive parameters in the model atmosphere.

Model parameter	Value
Albedo, α	10%
Terrestrial roughness length, z_0	0.4 m
Mean latitude, Φ	45°
Julian day	155
Synoptic surface pressure, P_{00}	1020×10^2 Pa
Synoptic specific humidity, q_{00}	0.01 g kg^{-1}
Zonal component of the large scale geostrophic wind, u_{gs}	1.89 m s^{-1}
Meridional component of the large scale geostrophic wind, v_{gs}	5.80 m s^{-1}
Soil diffusivity	3.0×10^{-7} m^2 s^{-1}
Soil density	1.5×10^3 kg m^{-3}
Soil specific heat capacity	1.34×10^{-3} J kg^{-1} K^{-1}
Soil wetness	10%
Initial height of PBL	1200 m

This can be shown through an evaluation of the meridional mesoscale geostrophic wind component v_{gm} based on the results of McNider and Pielke (1981). Using their representation for the equations of motion, we can write the zonal momentum equation as

$$\frac{du}{dt} = fv - fv_{gs} - \tilde{\theta}\frac{\partial \tilde{\pi}}{\partial x}, \tag{1}$$

where v_{gs} is the meridional component of the synoptic geostrophic wind. The variable v represents the observed meridional wind component and $\partial\tilde{\pi}/\partial x$ is equivalent to the mesoscale horizontal pressure gradient, as shown by McNider and Pielke (1981). The superscript tilde indicates that the variable represents the sum of a base state value which is dependent upon height and a mesoscale deviation from the base state. The synoptic deviation from the base state is included in the fv_{gs} term.

From (1) the mesoscale geostrophic wind component may be defined as

$$v_{gm} = \frac{\tilde{\theta}}{f}\frac{\partial \tilde{\pi}}{\partial x}, \tag{2}$$

so that the total geostrophic wind is $v_{gt} = v_{gm} + v_{gs}$. As described by McNider (1981) and McNider and Pielke (1981), it is the inertial oscillation of the wind about the total geostrophic wind that aids in explaining the preference for a nocturnal low-level jet maximum over the Great Plains at night.

The hydrostatic equation can be written as

$$\partial\tilde{\pi}/\partial z = -g/\tilde{\theta}. \tag{3}$$

By differentiating (3) with respect to x and reversing the order of the differentials we obtain

$$\frac{\partial}{\partial z}\frac{\partial \tilde{\pi}}{\partial x} = \frac{g}{\tilde{\theta}^2}\frac{\partial \tilde{\theta}}{\partial x} = \frac{g}{\tilde{\theta}}\frac{\partial \ln\tilde{\theta}}{\partial x}, \tag{4}$$

which may be combined with the vertically differentiated form of (2) to yield the vertical gradient of the mesoscale geostrophic wind,

$$\frac{\partial v_{gm}}{\partial z} = \frac{v_{gm}}{\tilde{\theta}}\frac{\partial \tilde{\theta}}{\partial z} + \frac{g}{f\tilde{\theta}}\frac{\partial \tilde{\theta}}{\partial x} = v_{gm}\frac{\partial \ln\tilde{\theta}}{\partial z} + \frac{g}{f}\frac{\partial \ln\tilde{\theta}}{\partial x}. \tag{5}$$

This form of the thermal wind equation is equivalent to that used by McNider (1981). Eq. (4) may also be

integrated between the surface and the top of the planetary boundary layer z_i to obtain

$$\left.\frac{\partial\tilde{\pi}}{\partial x}\right|_{z_i} - \left.\frac{\partial\tilde{\pi}}{\partial x}\right|_0 = g\int_0^{z_i}\frac{1}{\tilde{\theta}^2}\frac{\partial\tilde{\theta}}{\partial x}\,dz, \tag{6}$$

which when used in conjunction with (5) is useful for examining the physical forcing behind the coastal jet.

1) Over land during the day

Eq. (6) may be rewritten in a more convenient form by making the assumption that the magnitude of the surface pressure drop is directly proportional to the pressure change aloft (Defant, 1951, and Pielke, 1981). Since Fig. 5a shows that the eastern extent of the baroclinic zone is limited by turbulent mixing over the land, the well-mixed condition is satisfied in that region so that (5) and (6) may be rewritten as

$$\frac{\partial v_{gm}}{\partial z} = \frac{g}{f}\frac{\partial \ln\tilde{\theta}}{\partial x}, \tag{7}$$

$$(1+\alpha)\left.\frac{\partial\tilde{\pi}}{\partial x}\right|_0 = -\frac{gz_i}{\tilde{\theta}^2}\frac{\partial\tilde{\theta}}{\partial x} = -\frac{gz_i}{\tilde{\theta}}\frac{\partial \ln\tilde{\theta}}{\partial x}, \tag{8}$$

where the relation $\partial\tilde{\pi}/\partial x|_{z_i} = -\alpha\partial\tilde{\pi}/\partial x|_0$ has been used. Since the acceleration of the surface zonal wind is related to the horizontal pressure gradient, (8) shows that its acceleration is directly proportional to the horizontal temperature gradient and to the depth of the mixed layer. By integrating (7) from the surface to the top of the mixed layer z_i we obtain

$$\begin{aligned} v_{gm}|_z &= v_{gm}|_0 + \frac{gz_i}{f}\left\langle\frac{\partial \ln\tilde{\theta}}{\partial x}\right\rangle \\ &= v_{gm}|_0 + \frac{gz_i}{f}\frac{\partial \ln\tilde{\theta}}{\partial x}, \end{aligned} \tag{9}$$

where the angle brackets indicate a vertically averaged quantity. In the mixed layer it is assumed that $\langle\tilde{\theta}\rangle = \tilde{\theta}$ so that (9) indicates that $v_{gm}|_0 < v_{gm}|_{z_i}$ provided that $\langle\partial \ln\tilde{\theta}/\partial x\rangle > 0$. Eq. (9) also shows that the magnitude of the meridional mesoscale geostrophic wind at the top of the mixed layer is directly proportional to the depth of the mixed layer and the magnitude of horizontal temperature gradient. By replacing the horizontal temperature gradient in (7) with (8), we obtain

$$\frac{\partial v_{gm}}{\partial z} = -(1+\alpha)\frac{\tilde{\theta}}{fz_i}\left.\frac{\partial\tilde{\pi}}{\partial x}\right|_0, \tag{10}$$

which illustrates that the mesoscale geostrophic wind shear varies linearly with height in the mixed layer and that it is inversely proportional to the depth of the mixed layer. As a final observation, it should be noted that the horizontal temperature gradient reverses its sign above the mixed layer (see Fig. 5a). Consequently, (7) suggests that the meridional mesoscale geostrophic wind will obtain a maximum at the mixed layer top.

Further insight may be gained by differentiating (9) with respect to time to obtain

$$\left.\frac{v_{gm}}{\partial t}\right|_{z_i} = \left.\frac{v_{gm}}{\partial t}\right|_0 + \frac{g}{f}\left(z_i\frac{\ln\theta}{\partial t\partial x} + \frac{\partial \ln\theta}{\partial x}\frac{z_i}{\partial t}\right). \tag{11}$$

East of the sea breeze front during the day, (10) and (11) suggest that there will be very little change in $v_{gm}|_{z_i}$ due to the horizontally homogeneous conditions ($\partial \ln\tilde{\theta}/\partial x \approx 0$) within the mixed layer. This result is found in the model simulations; see Fig. 5a.

2) Over water during the day

Over the ocean, $|\partial\tilde{\theta}/\partial x| \neq 0$ but changes in the height of the mixed layer are small so that (11) may be written as

$$\left.\frac{\partial v_{gm}}{\partial t}\right|_{z_i} = \left.\frac{\partial v_{gm}}{\partial t}\right|_0 + \frac{gz_i}{f}\frac{\partial^2 \ln\tilde{\theta}}{\partial t\partial x}. \tag{12}$$

Note in Fig. 5a that a shallow, well mixed layer exists over the ocean due to the strong vertical shear of the large scale meridional wind component. Eq. (12) indicates that an increase of the southward velocity with time will occur provided the mean horizontal temperature gradient in the atmospheric mixed layer over the ocean is decreasing with time. An analysis of the model results in Fig. 6 shows that this is indeed the case and the result is the development of a southward coastal jet at hour 14.3 (LST) in Fig. 5a.

3) Over land after radiative sunset[4]

After radiative sunset, which occurs between 1 and 2 h before astronomical sunset at hour 18.7 (LST), terrestrial and radiative cooling combine with the inland advection of marine air to extend the baroclinic zone eastward. Prior to this, turbulent mixing due to terrestrial heating confined the baroclinic zone to a narrow region near the coast. When net radiative cooling begins over the land the amount of turbulent mixing is reduced due to stabilization of the lower atmosphere. In this case the analysis of (5) and (6) is complicated by the reduced amount of turbulent mixing in the terrestrial atmosphere. By utilizing the mean value theorem of calculus the following equivalent form of (8) can be derived:

[4] For the purpose of this paper "radiative sunset" is defined as that point in time when radiative cooling first exceeds turbulent convective heating at the surface in the absence of clouds. The radiative sunset is expected to vary spatially. In these simulations, the variation is small since the boundary layer is horizontally homogeneous to the east of the thermal front. This homogeneity results from uniform surface properties and the absence of topographic features.

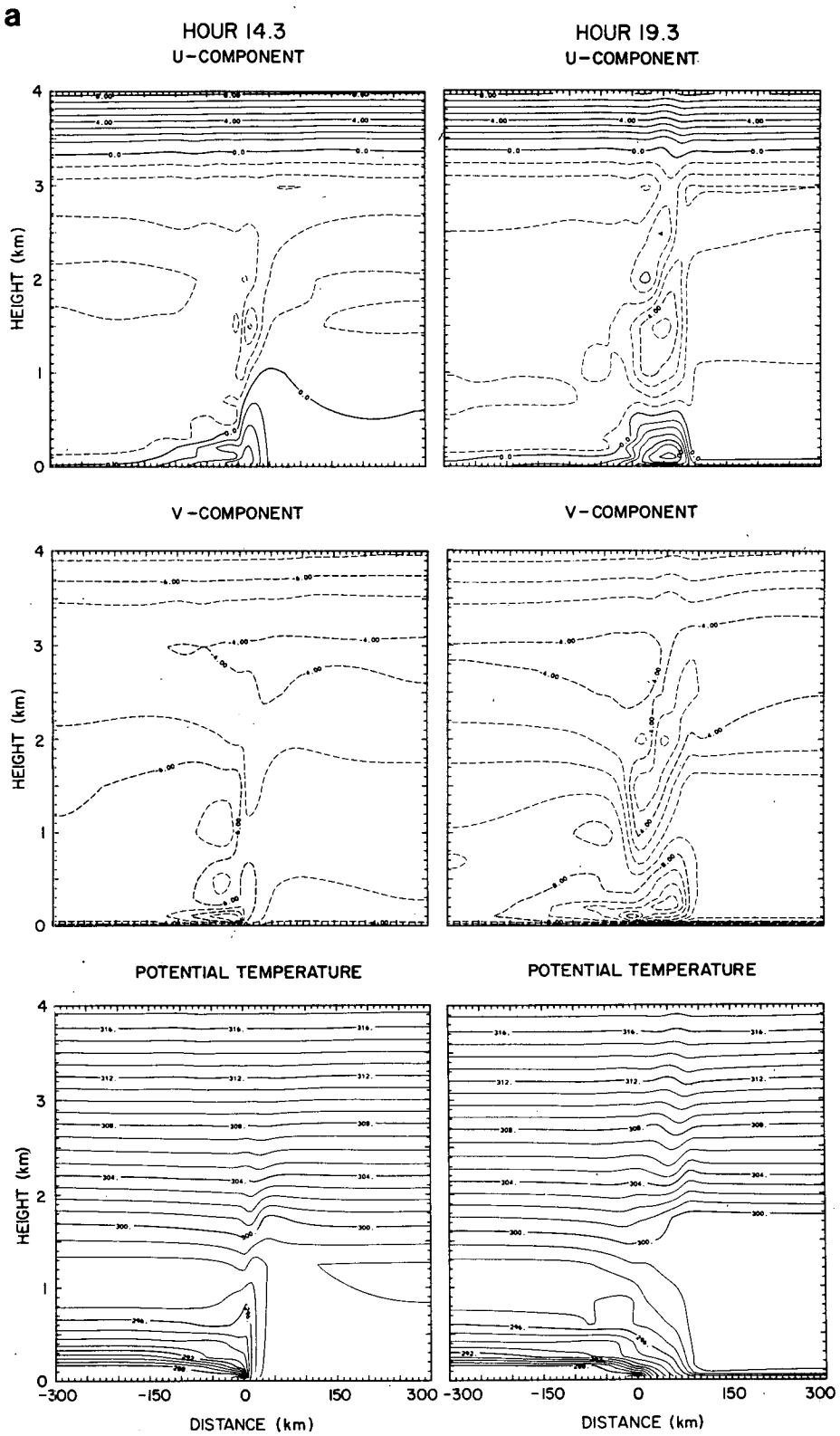

FIG. 5. The x–z contours of the u, v, and θ fields for the flat grid simulation in which the sea surface temperature is uniformly 289 K (contour intervals, 1 m s^{-1} and 1 K). (a) Hours 14.3 and 19.3 LST;

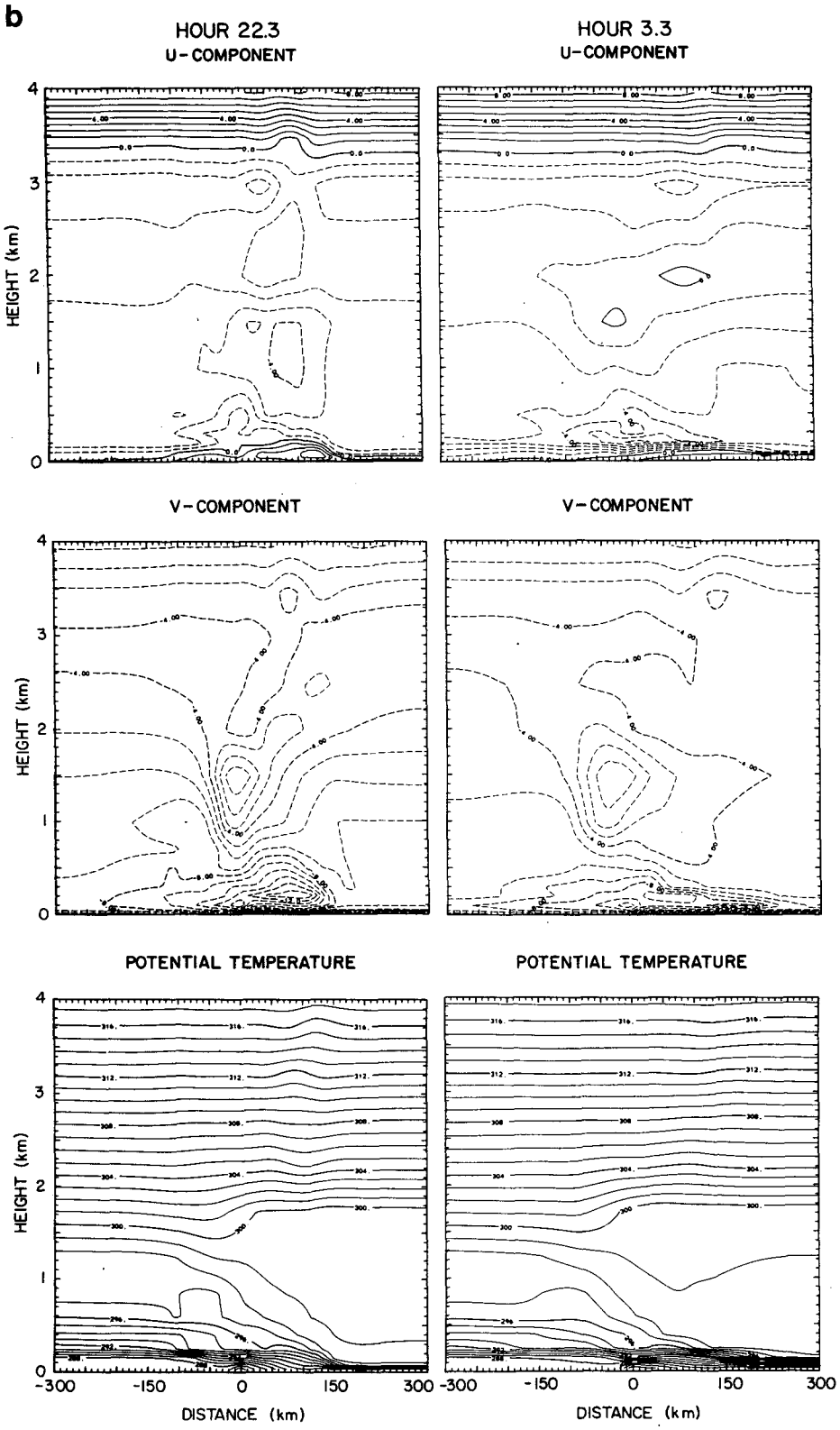

FIG. 5. (*Continued*). (b) hours 22.3 and 3.3 LST.

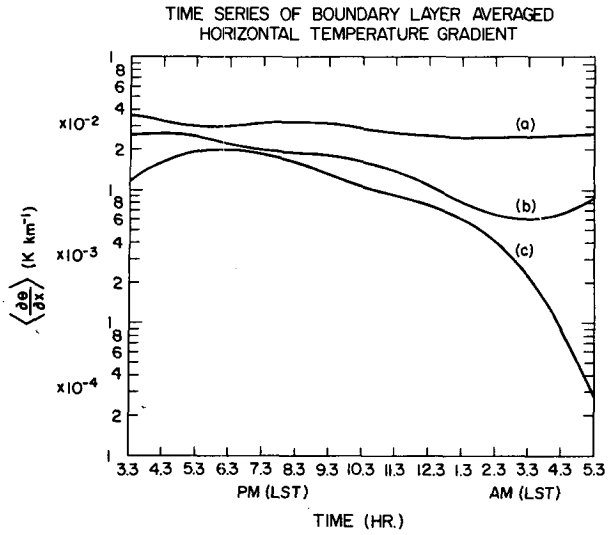

FIG. 6. Time series of the boundary layer averaged horizontal temperature gradient for three marine points, (a) 14 km offshore, (b) 30 km offshore and (c) 50 km offshore.

$$(1 + \alpha^*)\left.\frac{\partial \tilde{\pi}}{\partial x}\right|_0 = -gz_i^*\left\langle \frac{1}{\tilde{\theta}^2}\frac{\partial \theta}{\partial x}\right\rangle = -gz_i^*\left\langle \frac{1}{\tilde{\theta}}\frac{\partial \ln\tilde{\theta}}{\partial x}\right\rangle . \quad (13)$$

In (13) the superscript * is applied to indicate that the nighttime proportionality constant and the height of the boundary layer are most likely different from the daytime values. Again, the angle brackets are used to indicate a vertically averaged quantity. Two additional conclusions may be drawn from this equation:

- Since the top of the stable boundary layer is generally lower than that of the convective boundary layer, i.e., ($z_i^* < z_i$), it is expected that an offshore pressure gradient will be smaller, resulting in a relatively weak land breeze component.[5]
- Since the top of the stable boundary layer is below the convective boundary layer, the sudden reduction in the amount of turbulent mixing is responsible for the removal of friction between z_i and z_i^*. This suggests that a jet maximum will occur at the height z_i since this is where the mesoscale pressure gradient is largest.

The onshore advection of marine air moves the eastern boundary of the baroclinic zone eastward. The western boundary of the baroclinic zone remains at the coast because the land is warmer than the ocean throughout much of the night. The combined effects of cooling and marine air advection create two major regions of maximum in the horizontal temperature gradient as seen in Fig. 7. The eastern extension of the baroclinic zone is responsible for the development of a second longshore jet over the land [see Fig. 5a at hour 19.3 (LST)]. The core of this eastern jet is elevated due to the increased frictional influence of the land surface.

Prior to radiative sunset a layer of near neutral thermal stability extended from the surface layer to the top of the terrestrial boundary layer (see Fig. 5a). Near the coast advection of marine air restricted the height of the inversion to much lower elevations than farther inland. Following the onset of radiative cooling, the terrestrial atmosphere above the surface layer that is not influenced by the advection of marine air remains neutrally stratified. In the coastal region, a surface inversion develops due to the advection of marine air which restricts vertical mixing and indirectly causes lower surface and low-level atmospheric temperatures than in the neutrally stratified regions to the east where a shallow radiatively induced inversion develops. Fig. 8 illustrates the less stable stratification as one moves eastward from the coast and through the sea breeze front, which is located ~100 km inland.

From Fig. 8 it should be noted that the surface temperature increases eastward reaching a maximum in the vicinity of the front since this is where the surface inversion is weakest. This result is in agreement with the observations of Schroeder *et al.* (1967) (along the coast of Oregon) and Wexler (1946) (along the coast of Senegal, West Africa). Similar results have also been obtained from numerical model simulations by Physick (1976) and Estoque (1961). When explaining this observation, many investigators have relied upon the work of Estoque (1961), whose explanation differs from that presented here. Estoque (1961) suggested that to the east of the front turbulent mixing is negligible because the winds are weak, while to the west of the front stronger winds are responsible for increased turbulent mixing which transfers heat away from the surface. He concluded that the air to the east of the front will remain warmer than that to the west.

The results from this study suggest an alternative

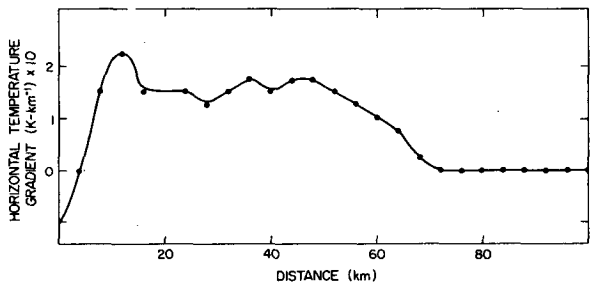

FIG. 7. A profile of the horizontal temperature gradient computed with space centered differencing at the 200 m level with an ocean surface temperature of 289 K at hour 19.3.

[5] Note that this feature is not seen in the model simulations since the ocean was not warm enough to force the development of a sufficient offshore mesoscale pressure gradient.

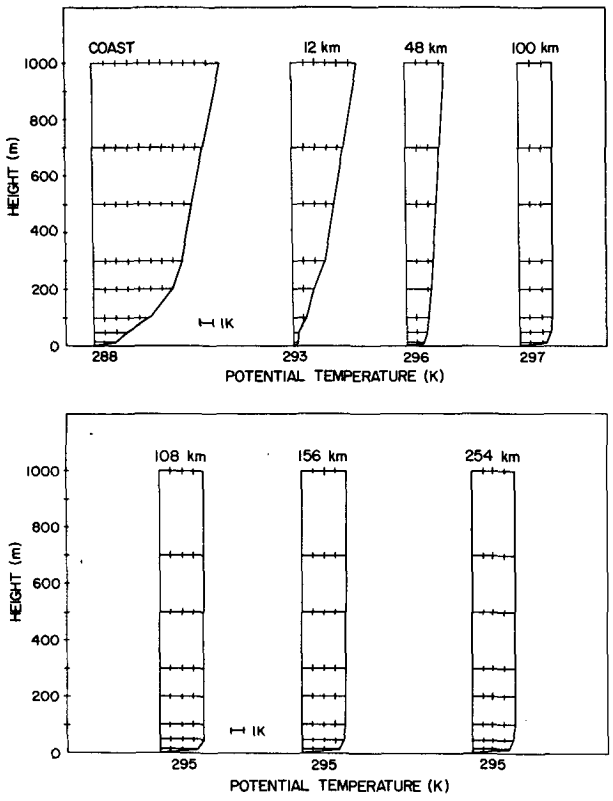

FIG. 8. Selected vertical profiles of potential temperature at hour 18.3 showing increased neutral stratification above the surface layer with movement toward the sea breeze front from the west with an ocean surface temperature of 289 K.

explanation. Fig. 8 shows that the region to the east of the front is less stably stratified above the surface layer than that to the west. This suggests that turbulent mixing is more active to the east of the seabreeze front, mixing heat downward toward the surface inversion. Here vertical shear of the horizontal velocity components is responsible for warming the surface by mixing air across the inversion. This explanation differs from that of Estoque (1961) in the following points:

- The effect of turbulent mixing is to warm the surface and lower atmosphere since the bulk of lower atmospheric cooling is due to long-wave radiative flux divergence near the surface.
- The inland regions to the east of the front undergo more turbulent mixing than those to the west due to the less stable thermal stratification above the surface layer.

One of the effects of the broader baroclinic zone discussed earlier is the horizontal displacement and intensification of the sea breeze core. This is the most common effect associated with the eastward advance of the baroclinic zone. This observation is seen in Fig. 5a at hour 19.3 (LST) where terrestrial cooling and the eastern advection of marine air combine to reduce the upper level offshore mesoscale pressure gradient at the western edge of the land. As a result the maximum mesoscale pressure gradient at the surface moves eastward with the baroclinic zone.

A secondary effect of the eastward extension of the baroclinic zone is the development of a second longshore jet as seen in Fig. 5a at hour 19.3 (LST). Both jets are forced by geostrophic adjustment to the horizontal temperature gradient. The analysis of this second jet is similar to that presented for the coastal longshore flow at hour 14.3 (LST) in Fig. 5a.

An important consequence of the increased stability is the creation of a shallower boundary layer and an attendant reduction in the depth to which the frictional influence of the surface impacts the free atmosphere. This effect is simulated in the atmospheric model by the inclusion of the local–nonlocal K formulation of McNider (1981). The most noticeable result of the reduction of the boundary layer depth is an intensification of the terrestrial longshore jet. Blackadar (1957) has shown that in the case where the effect of friction is instantaneously removed, the deviation from geostrophy follows the equation

$$A = A(t_0)e^{-if t}, \tag{14}$$

where $A \equiv (u - u_g) + i(v - v_g)$. Eq. (14) describes the inertial oscillation of the wind vector about the frictionally balanced state as a circle in the complex plane. The period η of this oscillation is $2\pi/f$. For the experiment reported here this oscillation is excited by a reduction of friction within much of the original convective boundary layer as the surface layer stabilizes. Since the results of experiments with the local–nonlocal K formulation of McNider (1981) have shown that turbulent mixing within the convective boundary layer approaches zero almost instantaneously after astronomical sunset it is expected that the strongest horizontal velocities will be observed around hour 23.0 (LST) or ~4 h after sunset. An examination of Fig. 9 reveals that the mesoscale wind component peaks around hour 23.3 (LST) which is in close agreement with the results from Blackadar's equation. This figure also shows that the nighttime reduction in the friction increases the amplitude of the mesoscale perturbation of the wind. These results are in agreement with the climatological results of Bonner (1969), who found that the highest percentage of summertime low-level jets for this region occurred around 2200 (LST).

The intensification of the longshore flow can be analyzed by returning to the vertical integration of (5). This time we cannot apply the well mixed approximation; however, by integrating (5) between the surface and the top of the mixed layer and applying the mean value theorem, we can write

$$v_{gm}|_{z_i} = v_{gm}|_0 + \langle v_{gm} \rangle \ln \frac{\tilde{\theta}(z_i)}{\tilde{\theta}(0)} + \frac{g z_i}{f} \left\langle \frac{\partial \ln \tilde{\theta}}{\partial x} \right\rangle, \tag{15}$$

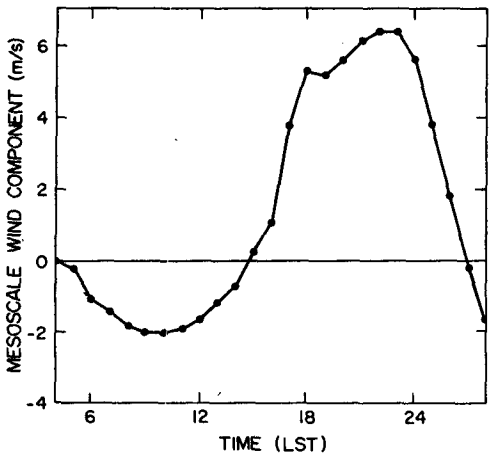

FIG. 9. The temporal variation of the mesoscale component of the wind at 300 m (AGL) for a point 48 km inland from the coast with an ocean surface temperature of 289 K.

where $\theta(z)$ represents the potential temperature at z. By differentiating (15) with respect to time we obtain

$$\left.\frac{\partial v_{gm}}{\partial t}\right|_{z_i} = \left.\frac{\partial v_{gm}}{\partial t}\right|_{0} + \frac{\partial \langle v_{gm}\rangle}{\partial t}\ln\left(\frac{\tilde{\theta}(z_i)}{\tilde{\theta}(0)}\right)$$

a b c

$$+ \langle v_{gm}\rangle \frac{\partial}{\partial t}\ln\left(\frac{\tilde{\theta}(z_i)}{\tilde{\theta}(0)}\right) + \frac{gz_i}{f}\frac{\partial}{\partial t}\left\langle\frac{\partial \ln\tilde{\theta}}{\partial x}\right\rangle$$

d e

$$+ \frac{g}{f}\frac{\partial \ln\tilde{\theta}}{\partial x}\frac{\partial z_i}{\partial t}. \quad (16)$$

f

When a transition between the convective and stable boundary layer is occurring, the height of the mixed layer top changes dramatically so that $\partial z_i/\partial t$ cannot be ignored and the analysis of (16) presented in Table 5 shows that each term in (16) contributes to the southward acceleration of the mesoscale geostrophic wind. Note that term (b) is not included in Table 5 because it was shown earlier that (a) and (b) are linearly related so there is no need to include (b) in the analysis. Since each of the terms (c) through (f) is negative, the mesoscale geostrophic wind will have a southward acceleration during the early evening (i.e., several hours after radiative sunset) when the magnitude of the time tendencies on the right hand side of (16) are greatest. During the late evening and early morning, portrayed in Fig. 5b at hours 22.3 (LST) and 3.3 (LST), the magnitudes of these time tendencies are smaller so that there is little change in the speed of the longshore, mesoscale geostrophic wind.

In Fig. 5b at hours 22.3 (LST) and 3.3 (LST) the terrestrial atmosphere becomes increasingly stable and less baroclinic. The increased stability is the result of long-wave radiational cooling. This reduction in the baroclinity weakens the sea breeze by reducing the onshore surface pressure gradient. Advection and weak turbulent mixing move the cool marine air inland weakening the horizontal temperature gradient throughout the night.

In conclusion the results of this experiment are in general agreement with the observational results from CUE I and with the theoretical results from previous investigators. In particular the results revealed:

- A daytime longshore jet that developed slightly offshore in response to the coastal baroclinity.
- The development of a terrestrial longshore jet as the sea breeze core moved onshore in response to a broadening of the baroclinic zone due to the continued eastward advection of marine air and a reduction in turbulent mixing after sunset.
- A nighttime longshore jet over the land which intensified as the frictional influence of the earth's surface was reduced due to the nighttime reduction of turbulent mixing within the boundary layer.

As a final point it should be noticed from Fig. 10 that the inland component of the daytime mesoscale circulation is contained within the boundary layer, while the upper level return flow is above the boundary layer. This feature is in agreement with the numerical

TABLE 5. An analysis of the components of Eq. (16).

Term	Components	Comments
c	$\ln[\tilde{\theta}(z_i)/\tilde{\theta}(0)] > 0$	Nocturnal boundary layer is stable.
	$\partial\langle v_{gm}\rangle/\partial t < 0$	The increasing high pressure offshore during the early evening results in a strong southerly wind.
d	$\partial\ln[\tilde{\theta}(z_i)/\tilde{\theta}(0)]/\partial t > 0$	Nocturnal boundary layer stratification increases with time.
	$\langle v_{gm}\rangle < 0$	The high pressure offshore results in a southerly mesoscale geostrophic wind component.
e	$\partial\langle\partial\ln\tilde{\theta}/\partial x\rangle/\partial t < 0$	The horizontal temperature gradient weakens with time after sunset.
f	$\partial z_i/\partial t < 0$	The height of the boundary layer decreases with stabilization of the boundary layer.
	$\partial\ln\tilde{\theta}/\partial x > 0$	The horizontal temperature gradient is positive because the land remains warmer than the water throughout the night.

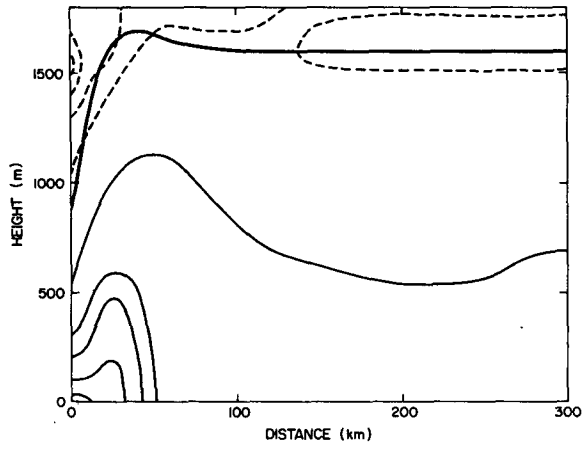

FIG. 10. The height of the planetary boundary layer (heavy solid line) at hour 14.3 (LST) plotted as a function of the distance inland from the coast with an ocean surface temperature of 289 K. Velocity contours of the transcoastal wind component are superimposed at intervals of 1 m s^{-1}.

results of Anthes (1978) as well as the CUE I observations of Johnson and O'Brien (1973). This organization results from the physical forcing behind the sea breeze. During the day terrestrial heating creates an onshore surface pressure gradient which drives the sea breeze. As the sea breeze moves across the coast, turbulent mixing redistributes the eastward momentum vertically. Since turbulent mixing is essentially confined within the convective boundary layer the eastward momentum of the sea breeze is mixed upward within the boundary layer and the upper level offshore flow is immediately above it.

b. *The upwelling ocean experiment*

This experiment is designed to examine the effect of upwelling on the mesoscale circulation. The spatial gradient of the sea surface temperature is prescribed as a space variant, time invariant boundary condition to the atmosphere. The spatial distribution of the sea surface temperature is displayed in Fig. 11. The results from this experiment are displayed in Fig. 12.

During the day these results (see Fig. 12a) show that the longshore flow is ~10% weaker than in the control simulation. It should also be noticed that the daytime onshore component of the mesoscale circulation has not increased its intensity in response to the surface temperature gradient (compare with Fig. 5a). The insensitivity of the sea breeze to the ocean thermal gradient is the result of two factors:

- As suggested by Clancy *et al.* (1979), the spatial scale of the ocean thermal gradient is not large enough to have a significant effect upon the mesoscale pressure gradient.
- The increased atmospheric stability associated with the area of the most intense upwelling retards the local atmospheric mixing necessary for the cold water to influence the mesoscale circulation.

From Figs. 11 and 12a it can be seen that $\partial\theta_s/\partial x < 0$ in the near coastal ocean where θ_s is the potential temperature of the surface layer. In the absence of coastal upwelling $\partial\theta_s/\partial x \geq 0$ because the land is warmer than the ocean and the ocean surface temperature is spatially uniform. As seen earlier this positive temperature gradient strengthens the longshore flow through geostrophic adjustment of the wind to the horizontal temperature gradient within the marine boundary layer. Consequently the negative horizontal thermal gradient found in Figs. 11 and 12a weakens the longshore flow through the same adjustment mechanism. At night there is no perceptible change in the intensity of the western core of the longshore flow. This result differs from that of Clancy *et al.* (1979) because their model showed a 3% increase in the strength of the mean longshore flow due to upwelling. This difference stems from the effect increased stability has upon the different atmospheric models. As reported by Clancy *et al.* (1979), upwelling reduced the thickness of their first atmospheric layer through cooling, thereby increasing the divergence of the vertical momentum flux. The net effect was to transport momentum downward, increasing the longshore flow. In our simulation the effect of upwelling is to increase the stability of the local atmosphere restricting the vertical momentum flux. Consequently, the jet is weaker than in the control experiment.

Figure 12a also shows that the daytime sea breeze does not increase its intensity in response to the ocean thermal gradient. This is a result of the increased stability associated with the advection of cooler marine air. Once the sea breeze core moves inland, it intensifies in agreement with the results of Clancy *et al.* (1979) and as observed in the previous section.

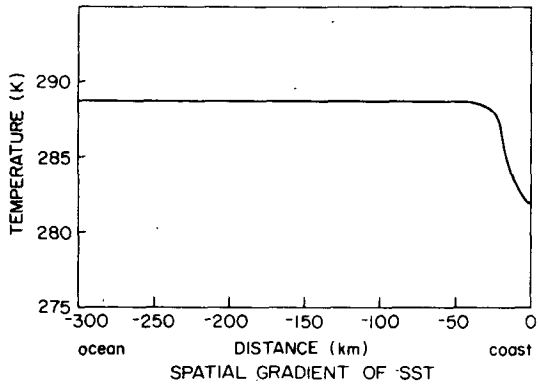

FIG. 11. The spatial gradient of sea surface temperature as predicted by the ocean model after seven days of integration and used as the ocean boundary condition in the spatial gradient sensitivity experiment.

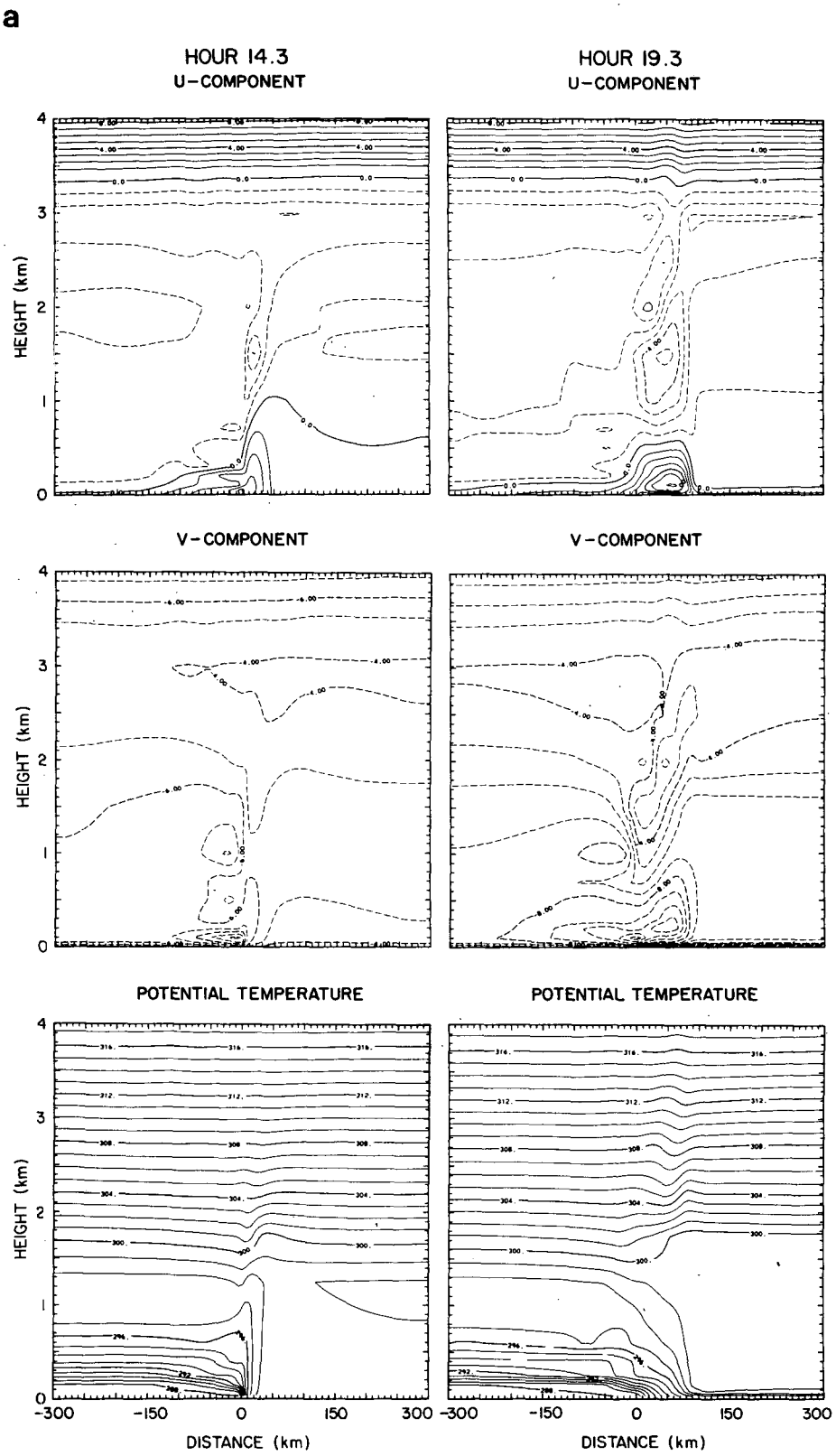

FIG. 12. As in Figs. 5a and b, except a spatial gradient of the sea surface temperature as described in Fig. 11 is used as the ocean boundary condition in this simulation (contour intervals, 1 m s^{-1} and 1 K). (a) Hours 14.3 and 19.3 LST;

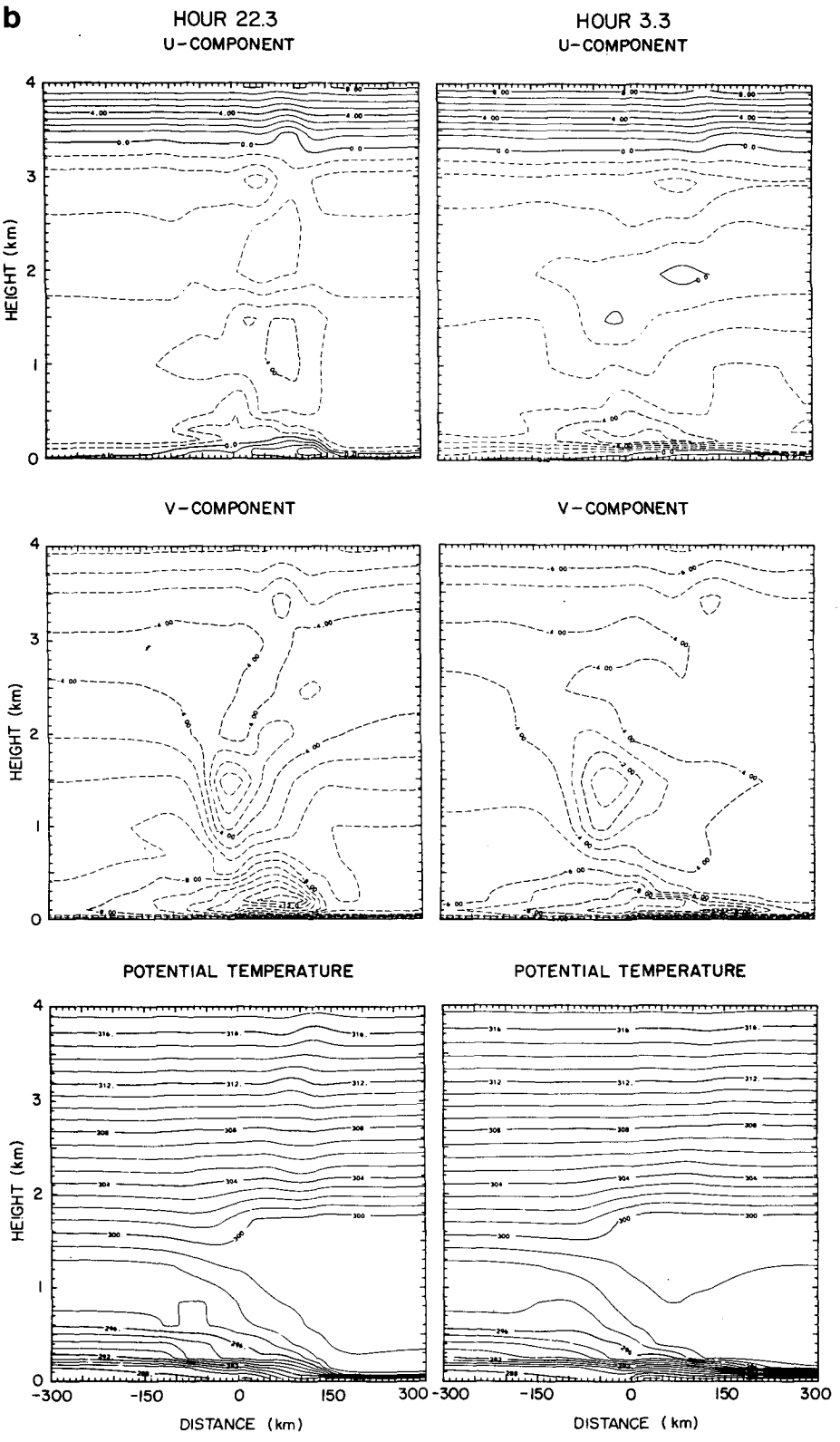

FIG. 12. (*Continued*). (b) hours 22.3 and 3.3 LST.

4. Summary and conclusions

Several mesoscale atmospheric phenomena were outlined in the introduction and a numerical mesoscale model was used as a research tool to examine these observed features. The results of the numerical simulations showed that:

- The surface onshore flow was confined below the main inversion and the return flow was found immediately above the inversion. This organization occurred because the eastward momentum is redistributed vertically by turbulent mixing within the boundary layer.
- The nocturnal low-level jet developed over the land in response to the sudden reduction in mixing within the boundary layer accompanying radiative sunset. Nighttime turbulent mixing falls off dramatically due to the stabilization of the lower atmosphere. The occurrence of this jet is consistent with the theoretical work of Blackadar (1957), the climatological work of Bonner (1968) and the field observations from the CUE I research program.

Our analysis of the model results also explained the following additional observations that were discussed in the text:

- The effects of terrestrial heating and turbulent mixing were found to overwhelm the inland advection of marine air so that there was no daytime thermal front east of the coast.
- After radiative sunset, the baroclinic zone broadened eastward in response to long-wave radiative cooling and subsequent stabilization of the lower atmosphere so that the marine air was advected inland with little modification.
- The warm zone to the east of the thermal front was maintained by downward turbulent mixing of mass toward the surface at night. The cool zone to the west of the front was maintained through the increased stability provided by the inland advection of cool marine air. This explanation differs from that of Estoque (1961), who suggested that the warm zone was maintained by reduced mixing and that the cool zone was maintained by mixing.
- During the day, upwelling weakened the longshore component of the wind. This effect was shown to be related to the increased atmospheric stability provided by the cool ocean waters resulting from upwelling and by the presence of warmer ocean surface to the west.

Acknowledgments. The authors would like to acknowledge the Atmospheric Sciences Section of the National Sciences Foundation (NSF) for their support under Grant 81073202. The model calculations were performed at the computing facility of the National Center for Atmospheric Research (NCAR) which is also sponsored by the NSF. We would also like to thank Richard McNider for his many comments and Jane Raese for her contribution on the word processor. Finally, Stephanie Honaski is acknowledged for drafting the figures.

REFERENCES

Anthes, R. A., 1978: The height of the planetary boundary layer and the production of circulation in a sea breeze model. *J. Atmos. Sci.*, **35**, 123–129.

Blackadar, A. K., 1957: Boundary layer wind maxima and their significance for the growth of nocturnal inversions. *Bull. Amer. Meteor. Soc.*, **38**, 283–290.

Bonner, W. D., 1968: Climatology of the low level jet. *Mon. Wea. Rev.*, **96**, 833–850.

Clancy, R. M., J. D. Thompson and H. E. Hurlburt, 1979: A model of mesoscale air–sea interaction in a sea breeze–coastal upwelling regime. *Mon. Wea. Rev.*, **107**, 1476–1505.

Defant, F., 1951: Local winds. *Compendium of Meteorology.* Amer. Meteor. Soc., 655–672.

Elliott, D. L., and J. J. O'Brien, 1977: Observational studies of the marine boundary layer over an upwelling region. *Mon. Wea. Rev.*, **105**, 86–98.

Estoque, M. A., 1961: A theoretical investigation of the sea breeze. *Quart. J. Roy. Meteor. Soc.*, **87**, 137–146.

Johnson, A., and J. J. O'Brien, 1973: A study of an Oregon sea breeze event. *J. Appl. Meteor.*, **12**, 1267–1283.

Lettau, H. H., and B. Davidson, 1957: Description and data takedown. *Exploring the Atmosphere's First Mile,* Vol. II. Pergamon, 201 pp.

Mahrer, Y., and R. A. Pielke, 1978: A test of an upstream spline interpolation technique for the advective terms in a numerical mesoscale model. *Mon. Wea. Rev.*, **106**, 818–830.

Mak, M. K., and J. E. Walsh, 1976: On the relative intensities of sea and land breezes. *J. Atmos. Sci.*, **33**, 242–251.

McCumber, M. C., and R. A. Pielke, 1981: Simulation of the effects of surface fluxes of heat and moisture in a mesoscale numerical model. 1. Soil layer. *J. Geophys. Res.*, **86**, 9929–9938.

McNider, R. T., 1981: Investigation of the impact of topographic circulation on the transport and dispersion of air pollutants. Ph.D. dissertation, Department of Environmental Sciences, The University of Virginia, 210 pp.

——, and R. A. Pielke, 1981: Diurnal boundary-layer development over sloping terrain. *J. Atmos. Sci.*, **38**, 2198–2212.

Mizzi, A. P., 1982: A numerical investigation of the mesoscale circulation in the Oregon coastal zone with a coupled atmosphere ocean model. M.S. thesis, Department of Environmental Sciences, The University of Virginia, 114 pp.

O'Brien, J. J., 1972: *CUE-I Meteorological Atlas.* Vol. 1. CUEA–IDOE Ref. M7265. Department of Meteorology and Oceanography, Florida State University, 309 pp.

Physick, W., 1976: A numerical model of the sea-breeze phenomenon over a lake or gulf. *J. Atmos. Sci.*, **33**, 2107–2135.

Pielke, R. A., 1981: An overview of our current understanding of the physical interactions between the sea and land breeze and the coastal waters. *Ocean Management,* **6**, 87–100.

——, and Y. Mahrer, 1978: Verification analysis of the University of Virginia three-dimensional mesoscale model prediction over South Florida for 1 July 1973. *Mon. Wea. Rev.*, **107**, 1568–1589.

Schroeder, M. J., M. A. Fosberg, O. P. Cramer and C. A. O'Dell, 1967: Marine air invasion of the Pacific coast: A problem analysis. *Bull. Amer. Meteor. Soc.*, **48**, 802–808.

Thompson, J. D., 1974: The coastal upwelling cycle on a beta-plane; hydrodynamics and thermodynamics. Ph.D. dissertation, Department of Meteorology, Florida State University, 141 pp.

Wexler, R., 1946: Theory and observation of land and sea breezes. *Bull. Amer. Meteor. Soc.*, **27**, 272–287.